# Radiance and Cloud Analyses from GOES-VAS Dwell Soundings

DONALD P. WYLIE AND HAROLD M. WOOLF

*Space Science and Engineering Center, University of Wisconsin—Madison, Madison, Wisconsin*

(Manuscript received 29 May 1999, in final form 15 November 1999)

ABSTRACT

An analysis technique for Geostationary Operational Environmental Satellite-VISSR (Visible and Infrared Spin Scan Radiometer) Atmospheric Sounder (GOES-VAS) sounder data was developed to extract cloud and clear radiance information. This technique employed many of the concepts used in the International Satellite Cloud Climatology Project (ISCCP) such as spatial and time comparisons of neighboring satellite pixels. It improved upon the previous studies that used VAS data by using all available VAS data at full time and space resolution. The previous studies utilized <10% of the original data.

The GOES-VAS cloud and clear radiance statistics compared well with rawinsondes and the ISCCP cloud analysis. The best agreement between the ISCCP and this GOES-VAS cloud analysis was for upper-tropospheric clouds (<440 hPa) in both cloud frequency and infrared emissivity. The two cloud datasets agreed to within 2% for both parameters. A comparison of the GOES-VAS clear radiance data to National Weather Service (NWS) rawinsondes showed agreement within 1.7 K (blackbody radiances). The upper-tropospheric VAS channels were warmer than the rawinsondes. The VAS water vapor channels suggested that the NWS rawinsondes have a dry bias in the upper troposphere.

## 1. Introduction

A central issue for the National Aeronautics and Space Administration's Mission to Planet Earth (Wielicki et al. 1995) is the construction of accurate datasets of the frequency, distribution, and changes of tropospheric clouds. These datasets are needed for the development of general circulation models (GCMs). Satellites provide the best data on upper-tropospheric clouds (Rossow and Schiffer 1999; Wang et al. 1996; Wylie and Menzel 1999) because of their downward view into the atmosphere. But the best upper-tropospheric cloud data come from polar-orbiting satellites, the National Oceanographic and Atmospheric Administration (NOAA) series, Stratospheric Aerosol and Gas Experiment (SAGE) II, and, in the future, earth observing system (EOS), Cloudsat, and Picasso-Cena. Polar orbiting satellites cannot follow changes in the diurnal cycles of clouds because they pass infrequently and view each location from different angles on each pass.

The Geostationary Operational Environmental Satellite (GOES) Visible Infrared Spin Scan Radiometer (VISSR) Atmospheric Sounder (VAS) has a dataset for which part of the earth was consistently observed 14 times per day. The GOES-VAS was the first atmospheric temperature sounding instrument flown on geostationary satellites (Smith et al. 1981). It originated in the mid-1970s, and NOAA has an archive of its data from 1978 to the present.

The VAS had 12 infrared channels from 3.95 to 14.7 $\mu$m in wavelength. Five channels were positioned in the longwave $CO_2$ absorption region from 13.3 to 14.7 $\mu$m for atmospheric temperature sounding with three additional channels for water vapor sounding at 6.7, 7.2, and 12.7 $\mu$m. The other four channels were in the shortwave infrared window and partial $CO_2$ absorption regions of the spectrum. In addition to temperature and moisture soundings, the VAS was also used for measuring sea surface temperature (Bates et al. 1987) and total column precipitable water (Chesters et al. 1987), assigning altitudes for cloud motion vectors (Menzel et al. 1983), and monitoring biomass burning (Prins and Menzel 1992).

The VAS provided a very sensitive means of detecting upper-tropospheric cirrus clouds (Wylie and Menzel 1989; Menzel et al. 1992; Schreiner et al. 1993), which are semitransparent to terrestrial radiation. The transparency of these clouds makes them difficult to detect using the channels common to weather satellites, which are typically a visible channel around 0.6 $\mu$m and a longwave infrared window channel around 11 $\mu$m. They are difficult to distinguish from lower clouds and the earth's surface because of infrared radiation penetrating through them. Yet, they are very important to radiative

*Corresponding author address:* Dr. Donald P. Wylie, Space Science and Engineering Center, University of Wisconsin—Madison, 1225 W. Dayton St., Madison, WI 53706.
E-mail: don.wylie@ssec.wisc.edu

cooling and heating of the troposphere. Global studies using a similar instrument on the polar-orbiting NOAA satellites report an average upper-tropospheric cirrus cloud coverage of 42% of the earth (Wylie et al. 1994; Wylie and Menzel 1999).

The VAS uniformly covers the diurnal cycle. The International Satellite Cloud Climatology Project (ISCCP; Rossow and Schiffer 1999) uses visible reflectance to identify cirrus clouds. The visible data in the ISCCP give very important information on the amount of solar energy reflected by clouds, which is a key component of the radiative heat budget. However, the ISCCP record lacks semitransparent cirrus detection and proper altitude assignment at night and where solar illumination angles are low. Because the VAS 13.3–14.7 $\mu$m channels have negligible solar reflection, monitoring infrared properties of the clouds is consistent through the diurnal cycle.

The GOES-VAS also has a long data record of nearly two decades. Coverage started in the late 1970s and continued to the 1990s. The new GOES satellites (Menzel and Purdom 1994) also continue with similar coverage by the GOES-Sounder instrument. This period covers three complete El Niño–Southern Oscillation (ENSO) events and a small drought in 1988. Two large volcanic eruptions spewed aerosol into the stratosphere that spread globally (Stowe et al. 1992). It should be noted that the stratospheric aerosol does not bias the cloud detection technique used here because the particles are too small to affect the 13.3–14.7 $\mu$m VAS channels.

This paper describes a prototype technique for detecting clouds and extracting infrared radiance information with the VAS data. This technique is more detailed than previous cloud studies that used VAS (Wylie and Menzel 1989; Menzel et al. 1992). Those studies sampled and averaged VAS data to a lower spatial resolution, using only 25% of the data. They also used only 4 of the 14 available VAS dwell sound[1] scans.

The cloud detection technique is discussed in section 2. The one-week dataset is described in section 3. A comparison is made to the ISCCP cloud products in section 4, and a comparison to rawinsonde soundings is shown in section 5. The diurnal cycle is discussed in section 6.

## 2. Method of analysis

The VAS data are analyzed in three steps. First a cloud mask is applied to identify the pixels with the highest confidence of being cloud free. Second, a uniform spatial analysis is made of the clear field of views (FOVs) for each channel so that the cloud height retrieval calculation has a clear radiance value for each cloudy pixel. Third, the radiative transfer equation, which requires a clear radiance estimate from the second step, is applied to calculate the height of the cloud and the infrared transmittance of the cloud. This is similar to the method described in Wylie and Menzel (1989) and its application to HIRS data in Wylie et al. (1994). This approach deviates from Wylie and Menzel (1989) in two ways: 1) the cloud mask does not depend on surface temperature data from an outside source; and, 2) this method uses every VAS pixel at the full resolution of the sensor, whereas Wylie and Menzel (1989) sampled and averaged the data thereby reducing the resolution.

### *a. Cloud mask*

The cloud mask is a critical component of the analysis because it affects several products that are extracted from the VAS data. Cloud heights and transmittances are calculated from a radiative transfer equation, which requires estimates of the cloud-free values for each channel. These calculations are discussed later in section 2c.

The cloud mask employs many of the same ideas used by the ISCCP (Rossow and Garder 1993). It examines space and time variations in the VAS data to find the FOVs most likely to be clear. It is more complicated than the previous techniques of Wylie and Menzel (1989) and Wylie et al. (1994). Those papers identified clear FOVs by comparing the 11-$\mu$m window channel blackbody radiative temperature to the surface temperature analyses of NOAA's National Center for Environmental Prediction (NCEP). FOVs within 2.5 K of the NCEP surface temperature, with allowance for water vapor attenuation, were marked as clear. The accuracy of the cloud detection technique was constrained by the limitations of the NCEP surface analysis. It did not have a diurnal cycle so satellite data were ignored during part of the day (Wylie et al. 1994), or an attempt was made to correct the NCEP analysis (Wylie and Menzel 1989; Menzel et al. 1992). This led to false indications of low clouds at night (Allis and Raman 1995a,b). The technique used here did not employ the NCEP surface temperature analysis; it was replaced by a base temperature derived from statistical properties of the VAS image.

A series of sequential tests was used to establish the base temperature. A spatial coherence test on the 11-$\mu$m window channel data was the first decision of the sequence. Coakley and Bretherton (1982) postulated that clouds would cause neighboring FOVs to differ in measured radiance because the clouds partially covered each FOV in different amounts. Thus neighboring FOVs should have similar radiances in clear areas because the only variations would be caused by the underlying surface.

Specifically, we grouped the 11-$\mu$m data into $2 \times 2$ FOV clusters and calculated the standard deviation of

[1] The instrument was made to ''dwell'' on a given scene by sampling the same line up to three times before moving the scan mirror, for the purpose of reducing radiometric noise.

the four FOVs in each cluster. All possible combinations of FOVs were used so that each single FOV appeared in four clusters. Clusters with 11-$\mu$m standard deviations $>0.45$ K (blackbody) over land and $>0.3$ K over water were deemed to contain clouds and were eliminated from the clear selection process. This decision was made for 1° latitude $\times$ 1° longitude cells over the study area, which extended from 25° to 50° north latitude and 40° to 130° west longitude.

Next, the average of the warmest 20% of the FOVs passing the spatial coherence test was used as the first approximation of the base temperature in each 1° $\times$ 1° square. Approximately 120 VAS FOVs were found in each 1° $\times$ 1° cell in the southeast part of the study area reducing to 60 FOVs in the northwest part. Two first approximations of base temperatures were saved for each 1° $\times$ 1° cell, one for land and a second for water. All four FOVs in the 2 $\times$ 2 clusters used in the spatial coherence test had to be from the same (land or water) domain.

The purpose of using the average of the warmest 20% instead of just the warmest cluster was to avoid anchoring the base temperature on noise from the instrument and from cloud contamination not previously detected. The warmest value in a region may not represent the mean conditions of the clear sky in the 1° $\times$ 1° cell. If an anomalously warm FOV were used, then some colder and clear FOVs might be omitted from the clear radiance analysis, leading to a warm bias in that quantity.

Because some clouds with uniform tops also could have passed the spatial coherence test, a test for consistency in time was made. The base temperature for each 1° $\times$ 1° cell was compared with the base temperatures on the day before and the day after at the same time of day. If agreement within 2.5 K with either the day before or after was found, then the base temperature was accepted as a best guess of the clear value. If no agreement was found with the day before or after, then the base temperature would come from the average of surrounding cells in a later step.

The time-comparison test identified changes in surface temperature caused by weather. A front moved through the southeastern United States during the week of VAS data used in this study (15–21 May 1988). This lowered the surface temperature as much as 10 K in some areas. Without the time-consistency test, we would have used only the warmest data that preceded the cold front and mistakenly missed the clear conditions following the front.

The time-consistency tests were made separately for land and water data. Hence one cell could have a valid base temperature for the water FOVs but not for the land FOVs. This situation occurred along coastlines.

A base temperature had to be derived for each cell for the cloud mask, so missing cells were filled with averages from surrounding base temperature data. The domain around the missing cell was progressively searched starting with the immediately adjacent eight cells. If seven cells were found with valid base temperatures, then the average was used for the missing cell. However, if seven could not be found then the search radius was expanded by one row and one column (1° latitude and longitude) looking for a minimum of seven valid base temperatures. The search was expanded in this manner until the seven were found. At the end of this process, all 1° $\times$ 1° grid cells in the study domain contained base temperatures.

The final clear/cloudy decision was made at each VAS FOV by comparing its 11.2-$\mu$m blackbody temperature to the base temperature. All VAS FOVs within 2.5 K of the base temperature were labeled as being clear; the others were processed for cloud height and emissivity. The clear pixels were averaged together in each 1° $\times$ 1° cell to form one clear radiance value for each of the 12 VAS channels. The clear/cloudy judgment was made with either the land or water base temperature value, depending on the location of the VAS FOV. To form one clear radiance value for each of the 11 VAS channels, the land and water values inside each 1° $\times$ 1° cell were averaged together.

### *b. The uniform clear radiance field*

Some of the 1° $\times$ 1° cells did not contain any clear VAS FOVs. This created a problem because clear values would be needed for each VAS channel in each 1° $\times$ 1° cell in the cloud height analysis (next step). The completely cloudy cells were given clear values from the seven closest cells with clear data using the same sequential search employed in establishing the base temperature fields. This gap-filling process was applied to all VAS channels.

### *c. Cloud height and emissivity*

The cloud height and infrared emissivity were calculated from the upwelling radiances measured by VAS channels using the same radiative transfer equation as Wylie and Menzel (1989) and Menzel et al. (1992). This equation uses VAS channels with partial $CO_2$ absorption, which makes the sounder channels sensitive to different levels in the atmosphere. The 13.3-$\mu$m channel has the least absorption so it ''sees'' farther into the troposphere than the 14.7-$\mu$m channel. Because of the layer sensitivity, this technique has been called the ''$CO_2$ Slicing Method.'' However, it is really based on the fact that a cloud will have a different contrast from the clear FOV radiance in each channel depending on three factors: 1) the depth in the atmosphere to which the channel can see, 2) the height of the cloud, and 3) the density of the cloud. Using any pair of $CO_2$ sounding channels, the radiative transfer equation can be simplified to the following form. A complete derivation of this equation is given in Wylie and Menzel (1989) and Wylie et al. (1994):

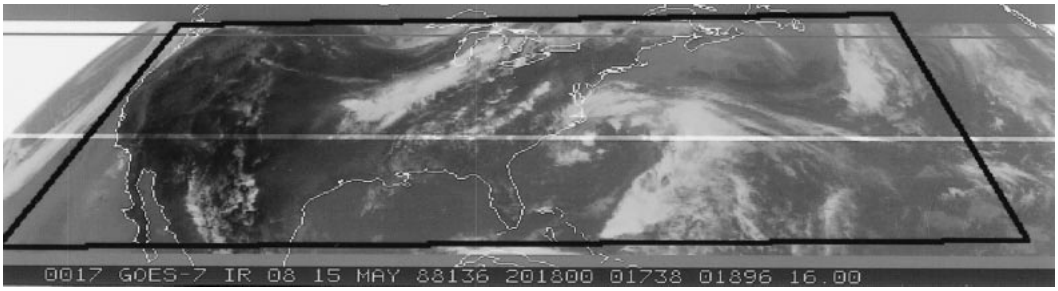


FIG. 1. One example 11.2-$\mu$m image made from two VAS dwell sound pairs at 2018 and 2038 UTC 15 May 1988. The white line is the overlap between the north (2018) and south (2048) dwell sounds. The black border is the boundary of the area studied, 25°–50° north and 40°–130° west.

$$\frac{R(\nu_1) - R\mathrm{clr}(\nu_1)}{R(\nu_2) - R\mathrm{clr}(\nu_2)} = \frac{N\epsilon_1 \int_{P\mathrm{sfc}}^{P\mathrm{cld}} \{\mathrm{Tr}(\nu_1, P)\partial B[\nu_1, T(P)]/\partial p\}\, dp}{N\epsilon_2 \int_{P\mathrm{sfc}}^{P\mathrm{cld}} \{\mathrm{Tr}(\nu_2, P)\partial B[\nu_2, T(P)]/\partial p\}\, dp}. \quad (1)$$

Here, $R(\nu_1)$ is the satellite measured radiance in channel $\nu_1$ and $R(\nu_2)$ is the radiance measured in channels $\nu_2$. Rclr($\nu_1$) and Rclr($\nu_2$) are the clear radiance values for those channels; Tr ($\nu$, $P$) is the transmittance from level $P$ to the top of the atmosphere; $\partial B(\nu, T(P))/\partial p$ is the vertical derivative of the Planck function for the channels; $N$ is the fraction of the cloud covering the FOV; and $\epsilon$ is the emissivity of the cloud.

The cloud height solution assumes that all attenuation of upwelling radiation by a cloud occurs at one level in the troposphere. A more realistic depiction requires knowledge of the vertical profile of cloud density; however, because clouds occur in a wide variety of vertical distributions, the single-layer assumption is the only method available for obtaining a unique solution. This approach is consistent with other algorithms proposed for detecting clouds using multispectral infrared sounders (Chahine 1974; McCleese and Wilson 1976; Smith and Platt 1978; Wielicki and Coakley 1981; Menzel et al. 1992; Susskind et al. 1997).

Equation (1) has only two unknowns, the cloud fraction-emissivity product ($N\epsilon$) and the pressure level of the cloud (Pcld). The transmittance and Planck functions are calculated from a vertical temperature profile. In this case we used a statistical sounding retrieval from the VAS data for the profile (see appendix). Because the channels are spectrally close, from 13.3 to 14.7 $\mu$m, we assume the $N\epsilon$ products are identical between channels ($\nu$) and cancel in Eq. (1). This leaves only one unknown, the cloud level pressure (Pcld). Both $R(\nu)$ and Rclr($\nu$) are taken from the satellite data. Pcld can be solved for directly without knowing the infrared emissivity of the cloud or the fractional cloud cover in the FOV ($N\epsilon$).

The $N\epsilon$ is later calculated from the 11-$\mu$m window channel radiances and the Planck function at the cloud level:

$$N\epsilon = \frac{R(11\ \mu\mathrm{m}) - R\mathrm{clr}(11\ \mu\mathrm{m})}{B[11\ \mu\mathrm{m}, T(P\mathrm{cld})] - R\mathrm{clr}(11\ \mu\mathrm{m})}. \quad (2)$$

For the lower-resolution HIRS sounder (20-km FOV diameter), two studies reported in Wylie et al. (1994) and Wylie and Menzel (1999) found that when $N\epsilon > 0.5$, $N \cong 1.0$ so $N\epsilon = \epsilon$. When $0.0 < N\epsilon < 0.5$, $N \cong \epsilon$.

The effective emissivity measurement, $N\epsilon$, also can be used to estimate an optical depth at visible wavelengths for comparison to other cloud data. By assuming that transmission is the complement of emission without scattering, the 11-$\mu$m infrared optical depth is

$$\tau_{11\mu\mathrm{m}} = \ln(1.0 - N\epsilon). \quad (3)$$

Visible optical depths ($\tau_{\mathrm{vis}}$) can be estimated from infrared window optical depths. Theoretical models of radiative scattering in clouds, reinforced by lidar and satellite measurements, indicate that the optical depth in the visible is about twice that at 11 $\mu$m (Platt 1979; Platt et al. 1987; Minnis et al. 1990; Wylie et al. 1995). We thus assume that

$$\tau_{\mathrm{vis}} = 2\tau_{11\mu\mathrm{m}}. \quad (4)$$

## 3. Example dataset

*GOES-7* satellite data were studied for seven days from 15 to 21 May 1988 (Fig. 1). The bounds of the area covered are 25°–50° north latitude and 40°–130° west longitude, which includes the continental United States, part of the Eastern Pacific Ocean, and part of the Atlantic Ocean. The GOES-VAS scanned this area in two 10-min periods one-half hour apart. The gray line in Fig. 1 is the overlap between the north and south VAS dwell sound images. The VAS dwell sound scans started at 48 and 18 min after the hour. Fourteen pairs of dwell soundings were analyzed from nominal times of 0103, 0233, 0403, 0533, 0703, 0833, 1003, 1303, 1433, 1603, 1733, 1903, 2033, and 2203 UTC. They were spaced at 1.5-h intervals except at 1133 and 2233

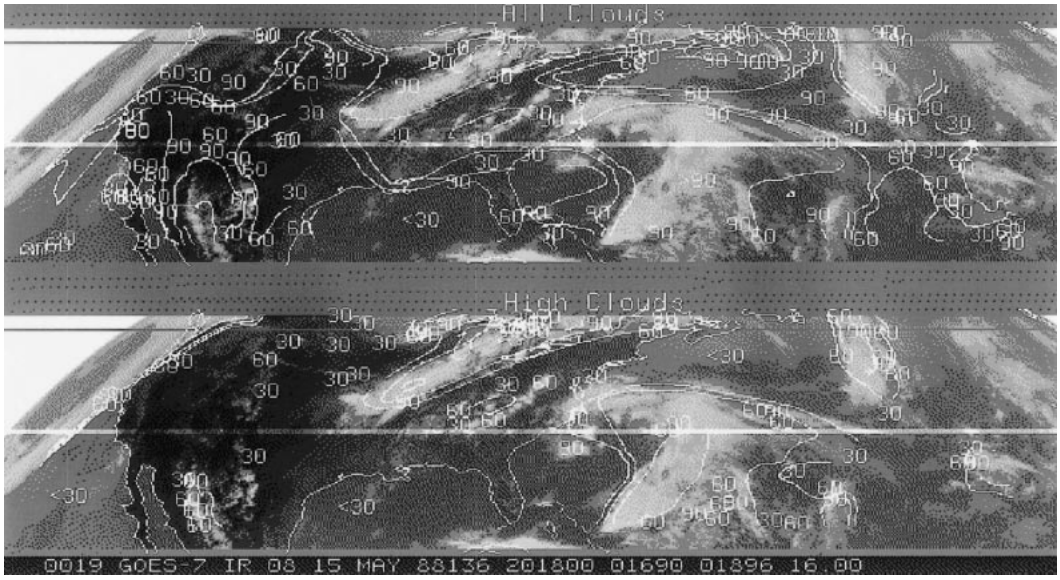


FIG. 2. The frequency or fraction of all clouds at all levels (upper panel) and the frequency of only high clouds above 440 hPa (lower) panel analyzed from the VAS dwell sound pair at 2018 and 2048 UTC.

UTC where the sounder scanned other areas away from the continental United States.

The infrared (11 $\mu$m) image is shown in Fig. 1; the frequency of all clouds (top panel) and high clouds above 440 hPa (bottom panel) is shown in Fig. 2. Clouds were found in 61% of the VAS data (Fig. 2); high clouds above 440 hPa were found in 29% of the data.

## 4. Comparison with the ISCCP

The ISCCP has analyzed data from most of the world's weather satellites for the last 16 yr. Radiance values from different satellites have been normalized to generate uniform datasets. The ISCCP has provided globally consistent cloud data that have been used extensively in other research.

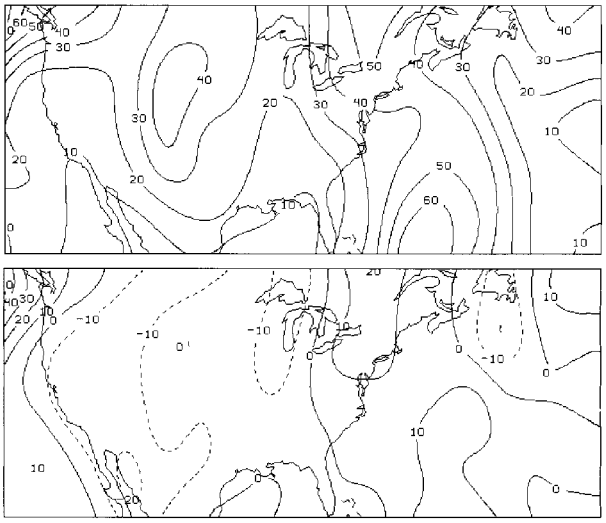

FIG. 3. The frequencies of high clouds <440 hPa averaged from 15–21 May 1988. Upper panel is the 7-day average from GOES VAS in percent, and the lower panel is the VAS-ISCCP difference.

The ISCCP D1 data were used. This dataset reported cloud statistics eight times per day in 3-h intervals starting with 0000 UTC. Because the ISCCP detection of high clouds requires solar reflection, we only used the ISCCP analyses at 1500, 1800, and 2100 UTC where solar illumination was present. The frequencies of clouds over the study area were averaged together. VAS data from similar times of 1433, 1603, 1733, 1903, and 2033 UTC were also averaged. The spatial pattern of the frequencies of clouds above 440 hPa is shown in Fig. 3 (upper panel) along with the difference of the VAS analysis from the ISCCP in the lower panel. Cloud frequencies agree within ±10% for most of the area. The VAS reported slightly lower cloud frequencies in the mountains of the western United States and higher values in the Bermuda region of the Atlantic Ocean. Overall the VAS cloud frequency averaged 83.7% over the area while the ISCCP averaged 72.2% (Table 1). For high clouds above 440 hPa, very close agreement was found with the VAS averaging 27.7% and the ISCCP averaging 28.3% (Table 1).

TABLE 1. Comparison of ISCCP and VAS cloud frequency averages. The study area spanned 25°–50°N and 40°–130°W and ran for 7 days from 15–21 May 1988.

| Cloud frequency (%) | All clouds all day | All clouds 15–21 UTC | Clouds > 440 hPa 15–21 UTC | N$\epsilon$ 15–21 UTC |
|---|---|---|---|---|
| ISCCP | 66.8 | 72.2 | 28.3 | 0.164 |
| GOES-VAS | 78.8 | 83.7 | 27.7 | 0.186 |

TABLE 2. The average N$\epsilon$ assigned to ISCCP $\tau_{vis}$ levels for Table 1.

| ISCCP category | $0.02 < \tau_{vis} < 1.27$ | $1.27 < \tau_{vis} < 3.55$ | $3.55 < \tau_{vis} < 9.38$ | $\tau_{vis} > 9.38$ |
|---|---|---|---|---|
| Average N$\epsilon$ | 0.24 | 0.65 | 0.91 | 1.00 |

The optical depths of the clouds also were compared using the relationships expressed in Eqs. (3) and (4). The ISCCP visible optical depths ($\tau_{vis}$) were converted to equivalent values of infrared $N\epsilon$ using the inverse form of (4):

$$N\epsilon_I = 1.0 - \exp(-\tau_{vis}/2). \quad (5)$$

The reason for converting the ISCCP data to $N\epsilon$, rather than converting VAS data to $\tau_{vis}$, is that $N\epsilon$ is linear in radiance whereas $\tau_{vis}$ is an exponential function of radiance. Also, the VAS analysis is limited by $N\epsilon$. When $N\epsilon > 0.95$, the corresponding $\tau_{vis} > 6$. Any greater $\tau_{vis}$ cannot be determined from the infrared VAS data.

The conversion was made using the six classes of $\tau_{vis}$ reported by the ISCCP. These classes cover a wide range from $\tau_{vis} > 0.02$ to $\tau_{vis} > 6.0$. We assigned mean values of $N\epsilon_I$ for the ISCCP $\tau_{vis}$ classes (Table 2) using the $\tau_{vis}$ divisions between their classes. For example, the lowest ISCCP class is $0.02 < \tau_{vis} < 1.27$. Now for $\tau_{vis} = 0.02$, $N\epsilon = 0.0$ and for $\tau_{vis} = 1.27$, $N\epsilon = 0.47$, so the first ISCCP class was assigned a mean $N\epsilon_I = 0.24$ (the subscript indicates ISCCP). The second class with $1.27 < \tau_{vis} < 3.55$ corresponds to $0.47 < N\epsilon < 0.83$. A mean value of $N\epsilon_I = 0.65$ was used for it. The frequency of clouds in each class was multiplied by the $N\epsilon_I$ for the class and summed over all ISCCP classes:

$$N\epsilon_1(\text{Total}) = \sum_{\text{Class}=1}^{6} N\epsilon_1(\text{Class}) \times \text{Freq(Class)}. \quad (6)$$

The VAS $N\epsilon$ averages were very close to $N\epsilon_I$. The $N\epsilon_I$ was only slightly lower at 0.164, compared to 0.186 for the VAS (Table 1). The close agreement in cloud frequency and $N\epsilon$ is surprising because no attempt was made to tune the VAS cloud mask to the ISCCP. The ISCCP D1 data were not examined until the VAS analysis had been completed.

## 5. Comparison with rawinsondes

The clear radiances measured by the GOES VAS were compared with channel radiances calculated from NWS soundings. The locations of the sounding stations are shown in Fig. 4. For the 0000 UTC NWS soundings two VAS dwell-sound groups were used: the 0103 UTC pair and the 2203 UTC pair from the previous day. For the 1200 UTC NWS soundings the 1003 and 1303 UTC pairs were used. The results of all four comparisons are shown in Table 3. The VAS dwell sound times were usually within 1.75 h of the rawinsonde times because the operational policy of the NWS is to launch their soundings from 30 to 45 min before the synoptic time listed for the data. Thus the 0000 UTC rawinsonde observations were made close to 2330 UTC, and the 1200 UTC observations near 1130 UTC. It takes about 2 h to complete a sounding to 10 hPa.

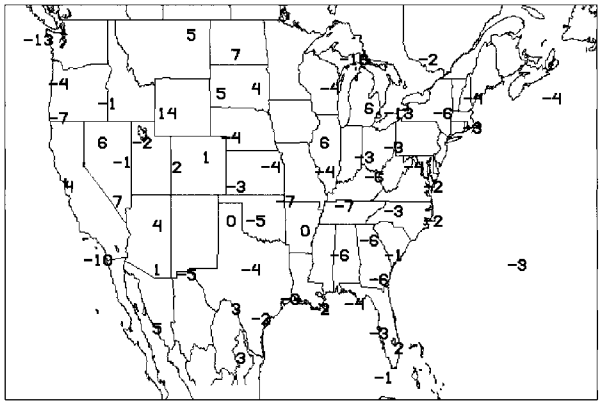

FIG. 4. The difference in radiances between the GOES-VAS measurement and calculated for the VAS 11.2-$\mu$m channel from rawinsondes averaged from 15–21 May 1988. The numbers have units of mw (m$^2$ sr cm$^{-1}$)$^{-1}$ rounded to the nearest integer and are at the locations of the rawinsonde stations.

For each sounding station, the VAS clear radiance data in the $1° \times 1°$ grid cell directly over it were used. Radiances for the VAS channels were estimated by applying the radiative transfer code described in appendix A to each temperature and moisture sounding. The average difference for the VAS 11.2-$\mu$m channel between the measured radiance and the estimate from the rawinsonde is the numeric value shown in Fig. 4 at each NWS rawinsonde location. The differences for the other channels averaged over all sounding locations are summarized in Table 3. Positive differences indicate the VAS measured clear radiances were warmer than those

TABLE 3. Radiance comparison between *GOES-7* VAS measurements and estimation of the radiances in the VAS channel calculated from National Weather Service rawinsonde data. 824 soundings from 71 stations over seven days from 15 to 21 May 1988 were used.

| VAS channel number | 3 | 4 | 5 | 7 | 8 | 9 | 10 |
|---|---|---|---|---|---|---|---|
| Wavelength ($\mu$m) | 14.2 | 14.0 | 13.3 | 12.7 | 11.2 | 7.3 | 6.7 |
| Average radiance [mw(m$^2$ sr cm$^{-1}$)$^{-1}$] | 47.6 | 59.3 | 92.6 | 113.0 | 102.3 | 15.0 | 7.1 |
| VAS measured − rawinsonde | | | | | | | |
| [mw(m$^2$ sr cm$^{-1}$)$^{-1}$] | +1.1 | +1.0 | −2.4 | −2.7 | −2.1 | −0.5 | −1.3 |
| (K blackbody) | +1.2 | +0.9 | −1.7 | −1.7 | −1.4 | −1.2 | −5.7 |
| Correlation coefficient of radiances | 0.03 | 0.26 | 0.72 | 0.84 | 0.83 | 0.58 | 0.46 |

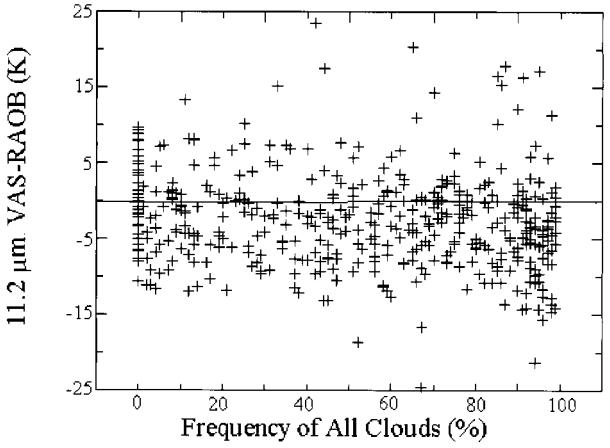


FIG. 5. The difference between GOES-VAS measured clear radiances at 11.2 $\mu$m and calculations of the same from rawinsonde temperature soundings plotted against the frequency of clouds from 15–21 May 1988.

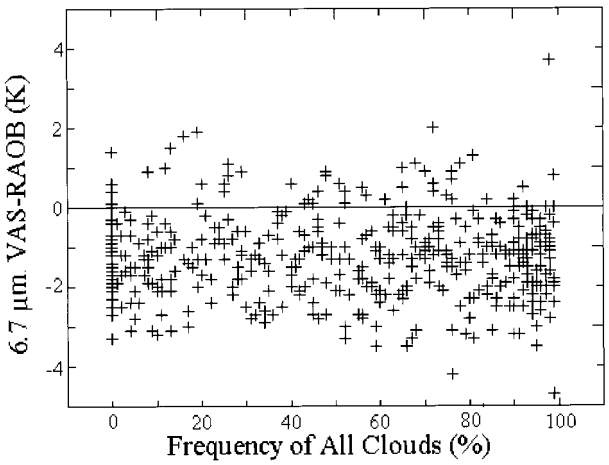


FIG. 6. The GOES-VAS measured radiance at 6.7 $\mu$m plotted against the frequency of clouds from 15–21 May 1988.

calculated from the soundings; negative differences indicate that the VAS clear radiances were colder.

VAS measured clear radiances appear to have biases associated with altitude. The higher-altitude channels, 3 and 4 (14.2 and 14.0 $\mu$m), averaged 0.9–1.2 K warmer than the calculations from rawinsonde soundings. The lower-altitude channels, 5, 7, and 8 (13.3, 12.7, and 11.2 $\mu$m), averaged 1.4–1.7 K colder than the sounding calculations. There are three likely causes for these discrepancies: biases in the VAS sensor calibration, errors in the cloud mask, and surface emissivity less than the assumed value of 1.0. If some low-level clouds, cumulus or stratus, were in the pixels labeled as clear FOVs, then a cold bias would be found. A warm bias, on the other hand, must be a result of calibration differences, given that it cannot be attributed to cloud contamination of the clear FOVs.

The VAS-rawinsonde differences for the 11.2-$\mu$m channel are examined as a function of cloud cover in Fig. 5. The VAS-rawinsonde difference does not show a relationship to cloud frequency. There appears to be more variance in the VAS-rawinsonde difference where cloud frequency was higher than in the clear and nearly clear areas. It should be noted that this comparison demanded that at least five clear FOVs be present in order to make a comparison with a rawinsonde sounding. This prevented the extrapolation of VAS clear radiance data into totally cloudy areas.

The water-vapor sensitive channels, 9 and 10 (7.3 and 6.7 $\mu$m), both had cold biases. The radiances in these channels are more affected by the moisture content of the upper troposphere than by temperature. A cold bias implies that the radiation reaching the satellite is coming from higher altitudes than expected from the rawinsonde sounding. This could be caused by the rawinsonde underreporting upper-tropospheric moisture, which commonly occurs, or from some cloud contamination in the VAS clear FOVs. Either situation would cause the same difference in this comparison. Given that the temperature channels (3 and 4) had a warm bias in the upper troposphere, cloud contamination does not appear to be a problem. The water channel biases are more likely due to reduced sensitivity of the rawinsondes in the upper troposphere.

The 6.7-$\mu$m channel difference is plotted against cloud frequency in Fig. 6. No relationship to cloud frequency is apparent, just as with the 11.2-$\mu$m channel. However, the 6.7-$\mu$m difference does have a strong relationship to the radiance in the channel itself (Fig. 7). The strong cold (or negative) bias appears mainly where the 6.7-$\mu$m radiance was high. These are the dry areas of the upper troposphere. In the wetter areas (lower 6.7-$\mu$m radiance), the VAS-rawinsonde difference is fairly evenly scattered around 0. This suggests that the rawinsondes may be underreporting upper tropospheric

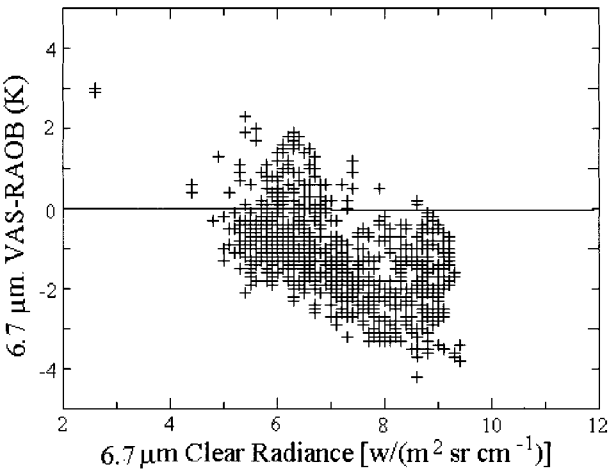


FIG. 7. The difference between the GOES-VAS measured radiances and calculations from rawinsondes at 6.7$\mu$m plotted as a function of the VAS measured radiance.

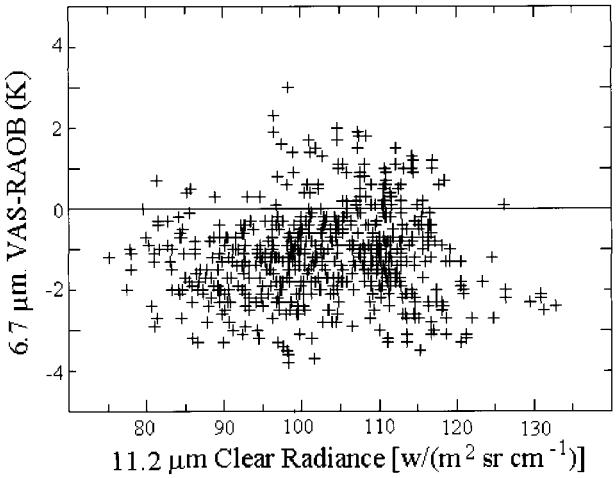


FIG. 8. The difference between the GOES-VAS measured 6.7-$\mu$m radiance and the rawinsonde calculation plotted as a function of the VAS measured 11.2-$\mu$m radiance.

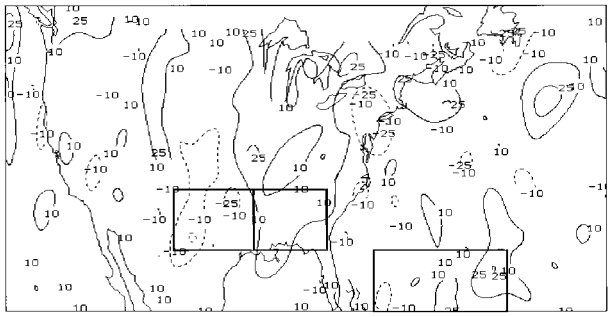

FIG. 9. The diurnal difference in frequencies of all clouds at all levels between the GOES-VAS dwell sounds at 1903 and 2033 UT minus the same from the dwell sounds at 0703 and 0833 UTC averaged from 15–21 May 1988. The boxes depict the locations or regional averages discussed in the text and shown in Figs. 11 and 13.

moisture in dry areas. No other cause is apparent, because the 6.7-$\mu$m differences do not show any relationship to the 11.2-$\mu$m radiances (Fig. 8) or cloud frequency.

## 6. Diurnal cycle

We looked at the diurnal variation of the VAS cloud frequency reports to assess the potential of these data in establishing diurnal cycles. We realize that seven days of data are too few to properly assess the diurnal cycles. However, one of the strengths of sounder data is its consistency during both day and night that other cloud detection schemes do not possess. A brief diurnal cycle analysis is given here with our seven-day dataset as an example of what could be done with the VAS archive.

The cloud frequencies from the VAS dwell-sounds in the late afternoon at 1903 and 2003 UTC were subtracted from the pre-sunrise dwell-sounds at 0703 and 0833 UTC (Fig. 9). Solar noon occurs at 1500 UTC on the eastern side of the study area (40°W) and at 2000 UTC on the western side (130°W). On the east coast of the United States, around 75°W, solar noon occurs at 1700 UTC. The 1903 and 2003 UTC dwell sounds thus cover about a 2-h period after solar noon.

Some differences in the frequencies of high clouds (<440 hPa) were found (Fig. 9). The differences in the southeastern United States were expected because of the growth in cumulus clouds. Another difference in the Atlantic Ocean was probably caused by movement of a front through the area and cannot be expected from a longer dataset. The cloud frequencies were averaged over three fairly large boxes as shown in Fig. 9. The Atlantic box covers 25°–30° N and 55°–75°W. The southeastern United States is bounded by 30°–35°N and 82°–93°W, covering the states of South Carolina, Georgia, Alabama, Mississippi, Tennessee, and part of Louisiana. The southwestern box covers 30°–35° N and 93°–105°W, which includes the states of Texas, Louisiana, New Mexico, and Oklahoma. These regions were chosen for their differences in diurnal variations as depicted in Fig. 9.

Plots of the high cloud frequencies for each of the 14 VAS dwell sound times in Fig. 10 show regular variations over the diurnal cycle. It should be noted that high clouds (<440 hPa) were more frequent in the southwestern box than in the southeastern box. This is contrary to the climate description of Menzel et al. (1992) and thus must be a consequence of the weather systems present during the short period studied.

The clear radiances in the 11.2-$\mu$m channel were also analyzed for their diurnal cycle. The differences of the 1903–2033 UTC dwell sounds from the 0703–0833 UTC dwell sounds are shown in Fig. 11. The largest differences are in the western United States, as expected. The ocean areas have small differences, if any. Some diurnal difference appears in the Pacific Ocean along the Baja coast of Mexico, which is probably due to the high cloud cover over the ocean. In areas where clear VAS FOVs were not found, the clear radiance values

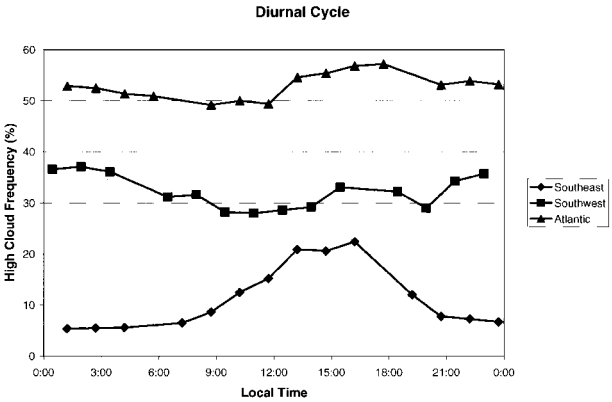


FIG. 10. The diurnal cycle in high cloud (>440 hPa) frequency for the three regions shown in Fig. 9.

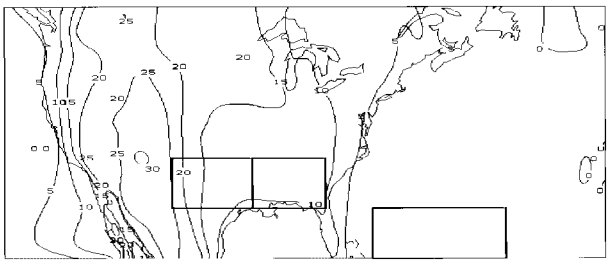

FIG. 11. The average blackbody temperature (°C) of the 11.2-$\mu$m VAS channel clear radiances from 15–21 May 1988. The boxes are the same local regions shown in Fig. 10.

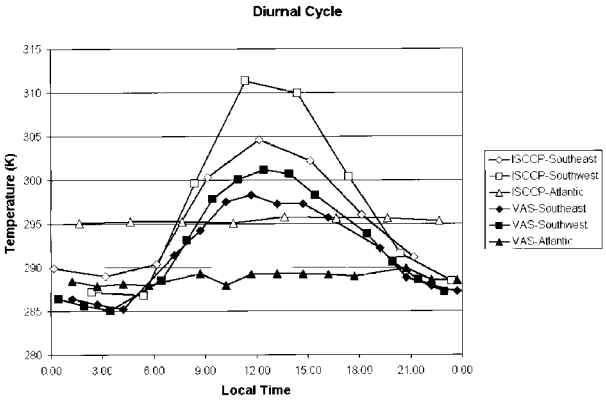


FIG. 12. The diurnal cycle of the VAS 11.2-$\mu$m blackbody clear blackbody temperatures in the regions shown in Fig. 12 along with the ISCCP surface temperature estimate for the same areas.

were extrapolated from neighboring analysis cells. Along the Baja coast, many of the oceanic cells had persistent cloud cover, so the clear radiance values assigned to them were influenced by averaging in some of the land data.

The blackbody temperatures were averaged over the same areas used for the high cloud diurnal study (Figs. 9 and 11). The averages at each of the 14 VAS dwell sound times are shown in Fig. 12 along with averages of the ISCCP surface temperature estimates. This graph shows a typical diurnal variation in temperature over land with little variation over the Atlantic box. Notice that the southwestern area has a higher afternoon temperature than the southeastern area, which is to be expected. The ISCCP surface temperatures are higher than the VAS data because the VAS data have not been corrected for water vapor attenuation in the window channel.

The time consistency between the 14 VAS analyses is apparent in Figs. 10 and 12. Time consistency is not forced by the cloud detection system described in section 2; it does not check preceding or succeeding VAS dwell sounds. It operates only on the VAS dwell sounds of the same time across several days. Each dwell sound time within a day is analyzed separately from the other times of the day. The smooth variations in Figs. 10 and 12 show that the VAS data can track diurnal variations. The fact that two of the cloud analyses show diurnal variations atypical of those expected from previous studies indicates that the variations measured here were probably caused by a single weather system that moved through the area during this short study. Clear radiance temperatures, however, did show typical diurnal cycles.

## 7. Summary and conclusions

We have shown that cloud detection using GOES-VAS sounder data has evolved beyond the studies of Wylie and Menzel (1989) and Menzel et al. (1992) by using statistical techniques similar to those of the ISCCP. Statistical relationships between satellite FOVs can be used to isolate the FOVs most likely to be cloud free. The spatial variance between neighboring pixels (spatial coherence) provided a good first step in eliminating cloudy FOVs. Further refinements came from looking for the warmest FOVs at each local time and comparing the warmest FOVs between successive days at the same time. The resulting cloud frequency and VAS channel clear radiance analyses exhibited typical diurnal variances with continuity between analysis times.

The cloud frequency analysis also had a surprisingly good agreement with the ISCCP analysis. The ISCCP uses slightly higher resolution data and a totally different method for altitude assignment of thin cirrus clouds that are partially transparent to terrestrial radiation. The sounders have typically found more upper-tropospheric clouds than the ISCCP (Jin et al. 1996). However, improvements have been made to the ISCCP since Jin et al. (1996). The present study showed very close agreement in the frequency of upper-tropospheric clouds and their radiative density over the area monitored by the GOES-VAS sounder. This agreement improves our confidence in the newer ISCCP data (Rossow and Schiffer 1999) and indicates that the sounder data can be used to extend ISCCP coverage into the night where the ISCCP's use of solar reflection data is not possible.

The clear radiance GOES-VAS dataset produced here agrees with rawinsonde data at a level similar to other programs that have monitored satellite performance. The differences between GOES-VAS clear FOV radiances and similar radiances estimated from NWS soundings averaged 1–1.7 K in blackbody temperature. The upper-tropospheric channels were slightly warmer ($\cong$1 K) than the rawinsondes. The VAS moisture channels also show a dry bias in the soundings in the upper troposphere.

*Acknowledgments.* This work was supported by Grants NAS13-98007, NAG5-4974, and 144-GS15 from NASA. The ISCCP data were electronically obtained from the NASA Langley Research Center DAAC. GOES-VAS data were obtained from the NOAA GOES archive.

## APPENDIX A

### Transmittance Modeling for VAS

*a. Line-by-line database*

Calculations have previously been done, using LBLRTM release 3.26 and HITRAN96 (Clough and Iacono 1995), for a set of 32 atmospheres, consisting of the *U.S. Standard Atmosphere, 1976,* and 31 diverse profiles representing a wide range of meteorological conditions, from arctic to tropical. The very high, variable spectral resolution output was reduced to uniform 0.1-wavenumber spacing by simple averaging. Four runs were made:

ALL, using the seven ''standard'' molecular species defined in LBLRTM—water vapor, carbon dioxide, ozone, nitrous oxide, carbon monoxide, methane, and oxygen;
WCO, water vapor continuum only;
WNC, water vapor with no continuum; and
WVO, water vapor (including continuum) plus ozone.

The calculations, which span the spectral range 550–2950 $cm^{-1}$, have been done for nadir view plus five zenith angles (theta) = 0., 36.87, 48.19, 55.15, 60., 63.61; the corresponding values of secant(theta) are 1.00, 1.25, 1.50, 1.75, 2.00, and 2.25.

*b. Generation of instrument transmittances*

The 0.1-wavenumber transmittances for the four absorber configurations described in section Aa were convolved with the response functions for the 12 bands or channels of the VAS instruments on *GOES-4* through *-7.* The resulting band transmittances were then subjected to the following operations:

$$\text{WET} = \text{WCO} \times \text{WNC}, \quad \text{OZO} = \text{WVO/WET}, \quad \text{and}$$

$$\text{DRY} = \text{ALL/WVO},$$

where DRY is a generic term applied to the remaining uniformly mixed gases, primarily carbon dioxide. Defining DRY and OZO(NE) in this manner preserves the validity of the product rule for total transmittance, even though the data do not actually represent monochromatic conditions.

*c. Fast (parameterized regression) model*

The transmittance profiles in each band were then used to generate separate sets of regression coefficients (for the constituents DRY, OZO, WCO, and WNC) employing the PLOD (Pressure Layered Optical Depth) algorithm (Hannon et al. 1996). In addition, a set of ''band-correction'' coefficients was generated to account for the polychromatic character of the bands or channels in calculating radiances and brightness temperatures. These procedures were performed for each of the four GOES-VAS instruments.

## APPENDIX B

### Statistical Retrieval Based on Synthetic VAS Brightness Temperatures

*a. Sounding database*

The basis for the statistical retrieval procedure is 14 months (December 1996–January 1998) of radiosonde data from the region 16°–60°N, 60°–130°W. The data were subjected to rigorous quality control and grouped in three-month overlapping sets: Dec–Feb, Jan–Mar, . . . , Nov–Jan. The number of soundings ranges from 11 921 in Feb–Apr to 12 931 in Jul–Sep, with the average around 12 400.

*b. Synthesis of radiometric data*

The ''forward model'' (fast transmittance algorithm plus related radiative-transfer code) was applied to each of the 12 sounding-data files, for each VAS instrument (*GOES-4* through *-7*), for the same six zenith angles utilized in the generation of the transmittance model.

*c. Regression procedure*

The brightness temperatures from section Bb were then regressed against the temperature and mixing ratio profiles described in section Ba, with secant(theta) as an additional ''channel,'' producing a four-satellite coefficient file for each of the three-month sounding datasets. The contents of these 12 files were then reorganized into a single file for efficiency of access.

## REFERENCES

Alliss, R. J., and S. Raman, 1995a: Quantitative estimates of cloudiness over the Gulf Stream locale using GOES VAS observations. *J. Appl. Meteor.,* **34,** 500–510.
——, and ——, 1995b: Diurnal variations in cloud frequency over the Gulf Stream locale. *J. Appl. Meteor.,* **34,** 1578–1594.
Bates, J. J., W. L. Smith, G. S. Wade, and H. M. Woolf, 1987: An interactive method for processing and display of sea-surface temperature fields using VAS multispectral data. *Bull. Amer. Meteor. Soc.,* **68,** 602–606.
Chahine, M. T., 1974: Remote sounding of cloudy atmospheres. I: The single cloud layer. *J. Atmos. Sci.,* **31,** 233–243.
Chesters, D., W. D. Robinson, and L. W. Uccellini, 1987: Optimized retrievals of precipitable water from the VAS split windows. *J. Climate Appl. Meteor.,* **26,** 1059–1066.
Clough, S. A., and M. J. Iacono, 1995: Line-by-line calculation of atmospheric fluxes and cooling rates. 2: Application to carbon dioxide, ozone, methane, nitrous oxide and the halocarbons. *J. Geophys. Res.,* **100,** 16 519–16 535.
Coakley, J. R., and F. P. Bretherton, 1982: Cloud cover from high resolution scanner data: Detecting and allowing for partially filled fields of view. *J. Geophys. Res.,* **87,** 4917–4932.
Hannon, S., L. L. Strow, and W. W. McMillan, 1996: Atmospheric infrared fast transmittance models: A comparison of two approaches. *Proc. SPIE,* **2830,** 94–105.
Jin, Y., W. B. Rossow, and D. P. Wylie, 1996: Comparison of the climatologies of high-level clouds from HIRS and ISCCP. *J. Climate,* **9,** 2850–2879.
McCleese, D. J., and L. W. Wilson, 1976: Cloud top height from

temperature sounding instruments. *Quart. J. Roy. Meteor. Soc.*, **102,** 781–790.

Menzel, W. P., and J. F. W. Purdom, 1994: Introducing GOES-I: The first of a new generation of geostationary operational environmental satellites. *Bull. Amer. Meteor. Soc.,* **75,** 758–781.

——, W. L. Smith, and T. R. Stewart, 1983: Improved cloud motion wind vector and altitude assignment using VAS. *J. Climate Appl. Meteor.,* **22,** 377–384.

——, D. P. Wylie, and K. I. Strabala, 1992: Seasonal and diurnal changes in cirrus clouds as seen in four years of observations with the VAS. *J. Appl. Meteor.,* **31,** 370–385.

Minnis, P., D. F. Young, K. Sassen, J. M. Alvarez, and C. J. Grund, 1990: The 27–28 October 1986 FIRE IFO cirrus case study: Cirrus parameter relationships derived from satellite and lidar data. *Mon. Wea. Rev.,* **118,** 2402–2425.

Platt, C. M. R., 1979: Remote sounding of high clouds: I. Calculation of visible and infrared optical properties from lidar and radiometer measurements. *J. Appl. Meteor.,* **18,** 1130–1143.

——, J. C. Scott, and A. C. Dilley, 1987: Remote sounding of high clouds. Part VI: Optical properties of midlatitude and tropical cirrus. *J. Atmos. Sci.,* **44,** 729–747.

Prins, E. M., and W. P. Menzel, 1992: Geostationary satellite estimation of biomass burning in South America. *Int. J. Remote Sens.,* **13,** 2783–2799.

Rossow, W. B., and L. C. Garder, 1993: Cloud detection using satellite measurements of infrared and visible radiances for ISCCP. *J. Climate,* **6,** 2341–2369.

——, and R. A. Schiffer, 1999: Advances in understanding clouds from the ISCCP. *Bull. Amer. Meteor. Soc.,* **80,** 2261–2287.

Schreiner, A. J., D. A. Unger, W. P. Menzel, G. P. Ellrod, K. I. Strabala, and J. L. Pellet, 1993: A comparison of ground and satellite observations of cloud cover. *Bull. Amer. Meteor. Soc.,* **74,** 1851–1861.

Smith, W. L., and C. M. R. Platt, 1978: Comparison of satellite-deduced cloud heights with indications from radiosonde and ground-based laser measurements. *J. Appl. Meteor.,* **17,** 1796–1802.

——, and Coauthors, 1981:First sounding results from VAS-D. *Bull. Amer. Meteor. Soc.,* **62,** 232–236.

Stowe, L. L., R. M. Carey, and P. Pellegrino, 1992: Monitoring the Mt. Pinatubo aerosol layer with *NOAA/11* AVHRR data. *Geophys. Res. Lett.,* **19,** 159–162.

Susskind, J. D., P. Piraino, L. Rokke, L. Iredell, and A. Mehta, 1997: Characteristics of the TOVS Pathfinder Path A dataset. *Bull. Amer. Meteor. Soc.,* **78,** 1449–1472.

Wang, P. H., P. Minnis, M. P. McCormick, G. S. Kent, and K. M. Skeens, 1996: A 6-year climatology of cloud occurrence frequency from Stratospheric Aerosol and Gas Experiment II observations (1985–1990). *J. Geophys. Res.,* **101,** 29 407–29 429.

Wielicki, B. A., and J. A. Coakley, 1981: Cloud retrieval using infrared sounder data: Error analysis. *J. Appl. Meteor.,* **20,** 157–169.

——, R. D. Cess, M. D. King, D. A. Randall, and E. F. Harrison, 1995: Mission to Planet Earth: Role of clouds and radiation in climate. *Bull. Amer. Meteor. Soc.,* **76,** 2125–2153.

Wylie, D. P., and W. P. Menzel, 1989: Two years of cloud cover statistics using VAS. *J. Climate,* **2,** 380–392.

——, and ——, 1999: Eight years of high cloud statistics using HIRS. *J. Climate,* **12,** 170–184.

——, ——, H. M. Woolf, and K. I. Strabala, 1994: Four years of global cirrus cloud statistics using HIRS. *J. Climate,* **7,** 1972–1986.

——, P. Piironen, W. Wolf, and E. Eloranta, 1995: Understanding satellite cirrus cloud climatologies with calibrated lidar optical depths. *J. Atmos. Sci.,* **52,** 4327–4343.